

A&A 580, A140 (2015)
 DOI: [10.1051/0004-6361/201425323](https://doi.org/10.1051/0004-6361/201425323)
 © ESO 2015

**Astronomy
&
Astrophysics**

Orbital phase-resolved spectroscopy of 4U 1538–52 with MAXI (Research Note)

J. J. Rodes-Roca^{1,2,3,*}, T. Mihara³, S. Nakahira⁴, J. M. Torrejón^{1,2}, Á. Giménez-García^{1,2,5}, and G. Bernabéu^{1,2}

¹ Dept. of Physics, Systems Engineering and Sign Theory, University of Alicante, 03080 Alicante, Spain
 e-mail: rodes@dfists.ua.es

² University Institute of Physics Applied to Sciences and Technologies, University of Alicante, 03080 Alicante, Spain

³ MAXI team, Institute of Physical and Chemical Research (RIKEN), 2-1 Hirosawa, Wako, Saitama 351-0198, Japan
 e-mail: tmihara@riken.jp

⁴ ISS Science Project Office, Institute of Space and Astronautical Science (ISAS), Japan Aerospace Exploration Agency (JAXA), 2-1-1 Sengen, Tsukuba, Ibaraki 305-8505, Japan

⁵ School of Physics, Faculty of Science, Monash University, Clayton, 3800 Victoria, Australia

Received 12 November 2014 / Accepted 10 July 2015

ABSTRACT

Context. 4U 1538–52, an absorbed high mass X-ray binary with an orbital period of ~ 3.73 days, shows moderate orbital intensity modulations with a low level of counts during the eclipse. Several models have been proposed to explain the accretion at different orbital phases by a spherically symmetric stellar wind from the companion.

Aims. The aim of this work is to study both the light curve and orbital phase spectroscopy of this source in the long term. In particular, we study the folded light curve and the changes in the spectral parameters with orbital phase to analyse the stellar wind of QV Nor, the mass donor of this binary system.

Methods. We used all the observations made from the Gas Slit Camera on board MAXI of 4U 1538–52 covering many orbits continuously. We obtained the good interval times for all orbital phase ranges, which were the input for extracting our data. We estimated the orbital period of the system and then folded the light curves, and we fitted the X-ray spectra with the same model for every orbital phase spectrum. We also extracted the averaged spectrum of all the MAXI data available.

Results. The MAXI spectra in the 2–20 keV energy range were fitted with an absorbed Comptonisation of cool photons on hot electrons. We found a strong orbital dependence of the absorption column density but neither the fluorescence iron emission line nor low energy excess were needed to fit the MAXI spectra. The variation in the spectral parameters over the binary orbit were used to examine the mode of accretion onto the neutron star in 4U 1538–52. We deduce a best value of $\dot{M}/v_\infty = 0.65 \times 10^{-9} M_\odot \text{ yr}^{-1}/(\text{km s}^{-1})$ for QV Nor.

Key words. X-rays: binaries – pulsars: individual: 4U 1538–52 – stars: mass-loss

1. Introduction

The high mass X-ray binary (HMXB) pulsar 4U 1538–52 has a B-type supergiant companion, QV Nor. The orbital period of the binary system is ~ 3.73 days (Davison et al. 1977; Clark 2000; Mukherjee et al. 2006), and the magnetised neutron star has a spin period of ~ 529 s (Davison et al. 1977; Becker et al. 1977). The distance to the source was estimated to be between 4.0 and 7.4 kpc (Crampton et al. 1978; Ilovaisky et al. 1979; Reynolds et al. 1992), and we use its latest estimation in this work: 6.4 kpc. Although an orbital low eccentricity was estimated to be $e \sim 0.08$, (Corbet et al. 1993), a higher value of $e \sim 0.17$ suggested an elliptical orbit for this system (Clark 2000; Mukherjee et al. 2006). Nevertheless, Rawls et al. (2011) argue that a circular orbit and an eccentric orbit cannot be distinguished. The X-ray luminosity is minimum during the eclipse that lasts ~ 0.6 days (Becker et al. 1977).

Both the timing and spectral properties of 4U 1538–52 have been studied with some X-ray observatories in different energy bands, such as Tenma (Makishima et al. 1987), EXOSAT (Robba et al. 1992), *Ginga* (Bulik et al. 1995), RXTE

(Clark 2000), *BeppoSAX* (Robba et al. 2001), *XMM-Newton* (Rodes-Roca et al. 2011), INTEGRAL (Hemphill et al. 2013), and *Suzaku* (Hemphill et al. 2014). The X-ray characteristics derived from these analyses suggest that the mass accretion onto the neutron star is consistent with a spherically symmetric stellar wind from the companion star (Mukherjee et al. 2006). The X-ray spectrum based on a broad band energy range has been described by different absorbed power-law relations, modified by a high-energy cutoff including a fluorescence iron line at 6.4 keV, whenever present, and with cyclotron resonant scattering features at ~ 21 keV (Clark et al. 1990; Robba et al. 2001) and at ~ 47 keV (Rodes-Roca et al. 2009). A soft excess component is found in the X-ray spectrum from *BeppoSAX* and *XMM-Newton* observations (Robba et al. 2001; Rodes-Roca et al. 2011). Similar to other wind-fed pulsars, the X-ray flux changes while the neutron star is moving in its orbit around the circumstellar environment of the companion star. Therefore, the variability is associated with the mass-loss rate by stellar wind captured by the gravitational field of the neutron star (\dot{M}). It also depends on the distance between both components and the stellar wind velocity, for the most part. The estimated X-ray luminosity is $\sim (2.6–9.1) \times 10^{36} \text{ erg s}^{-1}$ in the 3–100 keV range, assuming an isotropic emission and a distance of 6.4 kpc

* J.J.R.R. thanks the Matsumae International Foundation Research Fellowship.

(Reynolds et al. 1992). Thus, the analysis of the X-ray spectrum from the neutron star at different orbital phases provides us the variability of the model parameters we can use to compare with accretion models.

The Monitor of All Sky X-ray Image (MAXI) presents both all-sky coverage and moderate energy resolution, which gives us the possibility to investigate the orbital light curves and the orbital phase-resolved spectra of 4U 1538–52. In this paper, we used MAXI data to study the light curves, the orbital phase averaged spectrum, and the orbital phase-resolved spectra of 4U 1538–52 in the 2–20 keV energy range. Contrary to previous studies that focus on specific orbital phases at specific times, the more than five years of MAXI data analysed in this work tend to smear out short time scale variations and give more weight to long-term accretion structures. We describe the observations and the data reduction in Sect. 2, present the timing analysis in Sect. 3, the spectral analysis in Sect. 4, and in Sect. 5 we summarise our results. All uncertainties are hereafter given at the 90% ($\Delta\chi^2 = 2.71$) confidence limit, unless otherwise specified.

2. Observations

MAXI is the first astronomical mission on the International Space Station (ISS; Matsuoka et al. 2009). MAXI attached to the Japanese Experiment Module-Exposed Facility (JEM-EF). It consists in two types of X-ray slit cameras. The main X-ray camera is the Gas Slit Camera (GSC; Mihara et al. 2011) operating in the 2–20 keV energy range. The second one is the Solid-state Slit Camera (SSC; Tomida et al. 2011) operating in the 0.7–7 keV energy range. The in-orbit performance of GSC and SSC is presented in Sugizaki et al. (2011) and Tsunemi et al. (2010), respectively.

Every hour and a half, MAXI covers almost the entire sky per ISS orbit. Therefore, the source is observed around 1 ks per day by MAXI. We accumulated the exposure time to extract the spectra with a high enough level of counts.

3. Timing analysis

We first obtained the MAXI/GSC 1-orbit light curve¹ of 4U 1538–52 from MJD 55 058 to MJD 56 821 (i.e. nearly 5 years) in the 2–20 keV energy band to estimate the orbital period of the binary system. Then, we searched for a period assuming a sinusoidal signal, and the error was obtained using the relations derived by Leahy (1987). Our result was $P_{\text{orb}} = 3.7285 \pm 0.0006$ days, which is consistent with the value given by Mukherjee et al. (2006) ($P_{\text{orb}} = 3.728382 \pm 0.000011$ days). Then we folded the light curves with the best orbital period to obtain energy-resolved orbital intensity profiles. The orbital phase reference is taken from Mukherjee et al. (2006) (see also Baykal et al. 2006), with the phase zero corresponding to mid-eclipse in Fig. 1.

The MAXI/GSC data used in our analysis were extracted by the MAXI on-demand process using a 1.6 degree radius circular region centred on the X-ray source position with an annulus background region where we excluded other bright sources in the field. In Fig. 1 we show the background-subtracted light curves for the MAXI/GSC camera, folded at the orbital period of ~ 3.73 days, in the energy ranges 2–4 keV, 4–10 keV, and 10–20 keV. We note that the X-ray flux during the eclipse is compatible with no counts in all the energy bands when taking the uncertainties into account.

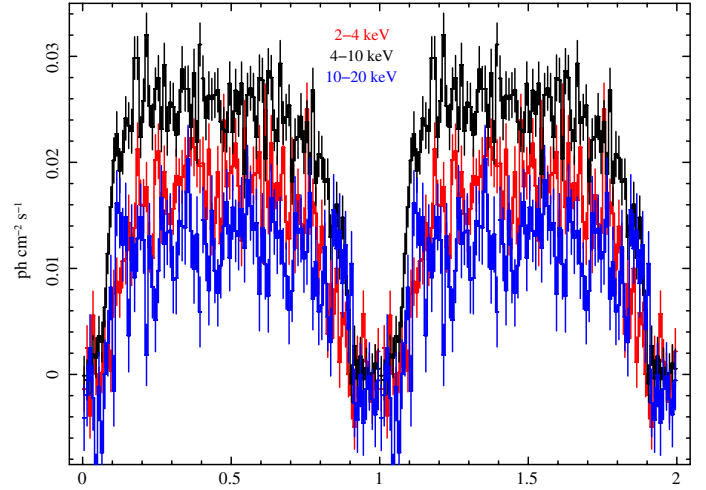


Fig. 1. MAXI orbital phase resolved background subtracted light curves of 4U 1538–52 in 2–4 keV, 4–10 keV, and 10–20 keV energy ranges using orbital parameters reported by Mukherjee et al. (2006), and then folded it relative to the mid-eclipse phase.

4. Spectral analysis

4.1. Orbital phase averaged spectrum

We extracted the orbital phase-averaged spectrum of 4U 1538–52 with MAXI/GSC for the same observation duration using the MAXI on-demand processing². For spectral analysis we used the XSPEC version 12.8.1 (Arnaud 1996) fitting package, released as a part of XANADU in the HEASoft tools. We used FTOOLGRPPHA to group the raw spectra as 2-133 channels by 4, 134-181 channels by 8, and 182-1199 channels by 12, so that all the spectral bins were Gaussian distributed. We tested both phenomenological and physical models commonly applied to accreting X-ray pulsars.

Comptonisation models attempt to provide a better physical description of the underlying emission mechanisms. We fitted the 2–20 keV energy spectrum with several successful models. We chose COMPST (in XSPEC terminology; Sunyaev & Titarchuk 1980) as the representative model, i.e., a Comptonisation of cool photons on hot electrons modified by an absorbing column along our line of sight. Because MAXI/GSC does not have enough sensitivity to detect the fluorescence iron emission line at ~ 6.4 keV, we have not needed to include it in our fits. The absorption column N_{H} fitted with other models were consistent, within uncertainties, and we use the COMPST values in the rest of this work. The soft excess at low energies (0.1–1 keV) presents in 4U 1538–52, and other HMXBs has not been considered here because it lies outside the energy range of the MAXI/GSC spectrum. Nevertheless, the well known fundamental cyclotron resonant-scattering feature (CRSF) at ~ 21 keV modifies the X-ray continuum above 16 keV (see references in Sect. 1). Therefore, we included the CRSF in our models and fixed its parameters with the values obtained by Rodes-Roca et al. (2009). We use the absorption cross sections from Verner et al. (1996), and the abundances are set to those of Wilms et al. (2000). The fitted parameters for the continuum model is listed in Table 1. In Fig. 2 we plot our data together with the absorbed COMPST best-fit model, and residuals of the fit as the difference between the observed flux and model flux divided by the uncertainty of the observed flux.

¹ MAXI homepage: <http://maxi.riken.jp>

² <http://maxi.riken.jp/mxondem>

Table 1. Fitted parameters for the MAXI spectra in Fig. 2.

Parameter	COMPST
N_{H} ($\times 10^{22}$ cm $^{-2}$)	4.9 ± 1.4
kT (keV)	$4.7^{+0.7}_{-0.5}$
τ	$17.8^{+2.4}_{-2.2}$
Norm ($\times 10^{-2}$)	2.7 ± 0.6
Flux (2–20 keV)	$6.5^{+0.3}_{-0.2}$
$\chi^2/\text{d.o.f.}$	40.6/43

Notes. A CRSF was included in the model (see text). Unabsorbed flux in units of ($\times 10^{-10}$) erg cm $^{-2}$ s $^{-1}$.

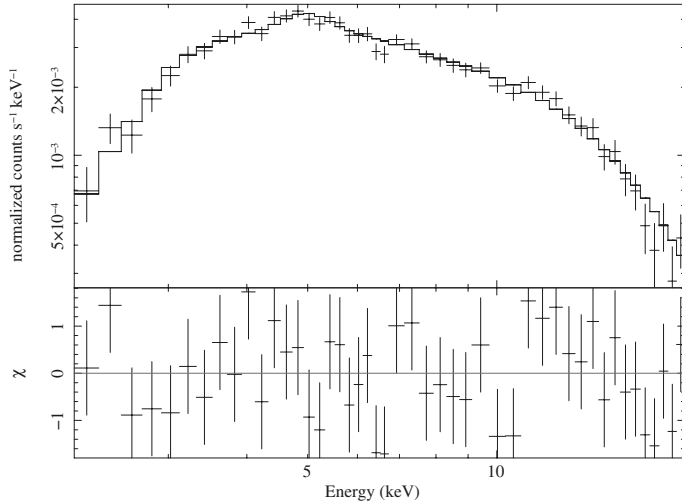


Fig. 2. Orbital phase-averaged spectrum of 4U 1538–52 in 2–20 keV band and X-ray model continuum modified by the fundamental CRSF. *Top panel:* data and absorbed Comptonisation of cool photons on hot electrons. *Bottom panel:* residuals between the spectrum and the model.

Since the total Galactic HI column density in the line of sight of 4U 1538–52 is in the $(9.14\text{--}9.70) \times 10^{21}$ atoms cm $^{-2}$ range (Dickey & Lockman 1990; Kalberla et al. 2005), the neutron star is moving almost all the orbit in additional absorbing material related to the stellar wind of the companion. Therefore, we studied its variability around the orbit extracting phase-resolved spectra in the next section.

4.2. Orbital phase-resolved spectra

Previous works in this direction have been carried out for only one or two orbits (Makishima et al. 1987; Robba et al. 2001; Mukherjee et al. 2006; Rodes-Roca 2007) or for a shorter orbital phase (Rodes-Roca et al. 2011). We obtained orbital phase-resolved spectra of the HMXB pulsar 4U 1538–52, accumulating the 60 s duration scans into six ~ 0.5 day orbital phase bins outside of eclipse (Nakahira et al. 2012; Doroshenko et al. 2013; Islam & Paul 2014).

In this analysis, we fitted the orbital phase-resolved spectra with the same model as we used in the orbital phase-averaged spectrum (see previous section). Although we also extracted the MAXI/SSC spectra, the time coverage of the SSC was too low to study spectral and flux changes. We therefore concentrated on the GSC data. For all the spectral models, we kept the parameters free, the orbital phase-resolved spectra were fitted from the energy ranges 2 keV to 20 keV. The range of the χ^2_{ν} values was 0.7–1.1 for all fits. Figure 3 shows the data, the absorbed

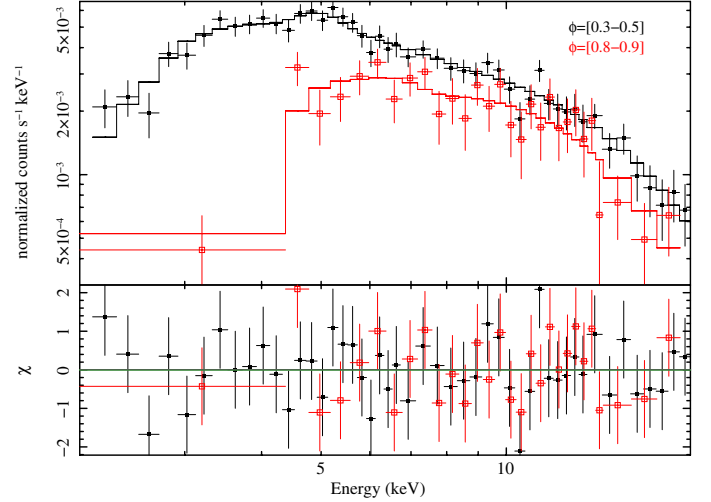


Fig. 3. Orbital phase-resolved spectra of 4U 1538–52 in the 2–20 keV band. *Top panel:* selected spectra and absorbed COMPST best-fit model. *Bottom panel:* residuals for the model.

Table 2. X-ray luminosity and Comptonisation parameter.

Orbital phase	L_{X} (10^{36} erg s $^{-1}$)	y
[0.1–0.2]	3.6	3.8
[0.2–0.3]	3.9	4.9
[0.3–0.5]	4.1	2.6
[0.5–0.7]	4.0	2.2
[0.7–0.8]	3.8	3.0
[0.8–0.9]	3.3	3.7

COMPST best-fit model, and residuals as the difference between observed flux and model flux divided by the uncertainty of the observed flux. We obtained six orbital phases to keep a good S/N ratio. In Fig. 3 we plot the highest and lowest flux spectra and two sets of residuals.

The variability of the spectral parameters for the absorbed thermal Comptonisation with a spherical geometry (COMPST in XSPEC) is shown in Fig. 4. The Comptonisation parameter, $y = kT \tau^2 / (m_e c^2)$, determines the efficiency of the Comptonisation process (Titarchuk 1994; Prat et al. 2008), and we derived its value from the six orbital phase ranges (see Table 2). This indicates an efficient process that corresponds to a moderate accretion rate, which is higher in the orbital phase ranges just before and after the eclipse than in the mid-orbital phase ranges. Moreover, it is consistent with similar observations of Vela X–1 performed by MAXI (Doroshenko et al. 2013). The unabsorbed flux along the orbit has no significant evolution, $(7.2\text{--}8.8) \times 10^{10}$ erg cm $^{-2}$ s $^{-1}$ in the fitting energy range (2–20) keV, showing that the accretion rate is quite stable in the phase bins considered.

4.3. The stellar wind in 4U 1538–52

One way to study the stellar wind in HMXBs is in terms of the variability of the equivalent hydrogen column density throughout the binary orbit. In fact, a simple spherically symmetric stellar wind model may describe the observed orbital dependence of the column density for certain range of the orbital inclination (Clark et al. 1994; Mukherjee et al. 2006; Rodes et al. 2008). To estimate the stellar mass-loss rate, the equivalent absorption column was derived by integrating the wind density along the

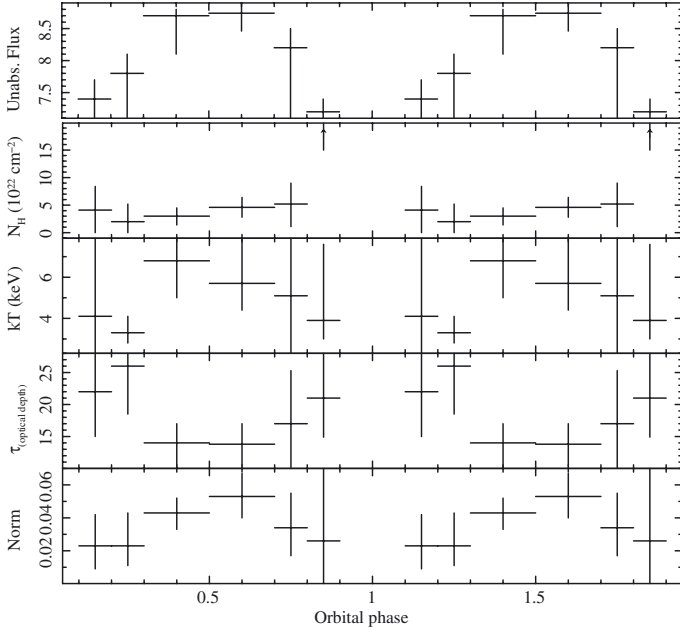


Fig. 4. Orbital phase changes in the free spectral parameters fitted in the 2–20 keV band. Spectral parameters are associated with the absorbed Comptonisation of cool photons by hot electrons (COMPST) model. Unabsorbed flux is in units of 10^{-10} erg cm $^{-2}$ s $^{-1}$.

line of sight to the X-ray source, that is, to combine the simple spherically symmetric wind model and conservation of mass equations. Then, the hydrogen number density at distance r from the donor, $n_{\text{H}}(r)$, can also be estimated through the following relationship:

$$n_{\text{H}}(r) = \frac{X_{\text{H}} \dot{M}}{m_{\text{H}} v_{\infty} (1 - R_{\star}/r)^{\beta} 4 \pi r^2} \quad (1)$$

with m_{H} the hydrogen atom mass, X_{H} the hydrogen mass fraction, \dot{M} the mass loss rate, v_{∞} the terminal velocity of the wind in the range 1400–2800 km s $^{-1}$ (Abbott 1982), where $r = 23.4 R_{\odot}$ represents the binary separation (Clark 2000). The parameter $\beta = 0.8$ – 1.2 is the velocity gradient for an OB supergiant (Friend & Abbott 1986), and $R_{\star} = 17.2 R_{\odot}$ (Reynolds et al. 1992), the radius of the donor. The resulting N_{H} arises from the integration of $n_{\text{H}}(r)$ along the line of sight. In Fig. 5 we show the equivalent hydrogen column density measured with MAXI as a function of the orbital phase.

The lines represent the model calculations of the absorption column density for different values of β and \dot{M}/v_{∞} ($M_{\odot} \text{ yr}^{-1}/\text{km s}^{-1}$) in units of 10^{-9} . The red line corresponds to $\beta = 0.8$ and $\dot{M}/v_{\infty} = 0.3$; the blue line corresponds to $\beta = 1.2$ and $\dot{M}/v_{\infty} = 0.3$; the green line corresponds to $\beta = 0.8$ and $\dot{M}/v_{\infty} = 3.0$; and the turquoise line corresponds to $\beta = 1.2$ and $\dot{M}/v_{\infty} = 3.0$. Our best least-squares fit is the black line, which corresponds to $\beta = 1.2$ and $\dot{M}/v_{\infty} = 1.3$. The value of the other orbital parameters have been taken from Clark (2000) and Mukherjee et al. (2006; see also Baykal et al. 2006). As can be seen, our data cannot distinguish between different values of β . We also note that our estimations of \dot{M}/v_{∞} did not change very much with the eccentricity and orbital inclination. None of the fits could describe all the experimental data. Consequently, we looked for the most useful upper and lower values of the fit. From the eclipse egress to the mid-orbit, the models with a lower \dot{M}/v_{∞} fit the data well (red and blue lines), but from the mid-orbit to the eclipse ingress, a higher value of \dot{M}/v_{∞} (green and turquoise lines) is required. This

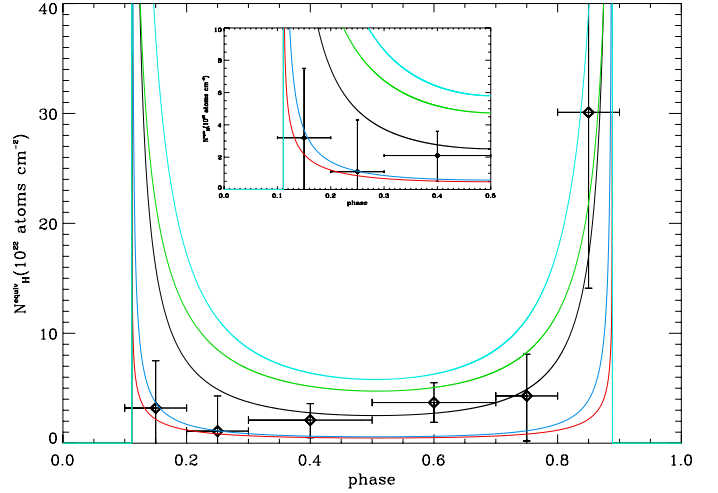


Fig. 5. Variation in column density versus orbital phase. Red, blue, black, green, and turquoise lines represent the wind model for different values of β and \dot{M}/v_{∞} . See text for details.

fact suggests that the neutron star is crossing an overdense region of the stellar wind and/or some trailing accreting material passing through the line of sight. Moreover, hydrodynamical simulations show that the interaction among the gravitational field of the neutron star, the radiation field of the X-ray source, and the stellar wind may lead to the formation of large structures of higher density compared to the unperturbed stellar wind (Blondin et al. 1990). These structures are formed mainly in the trail of the neutron star. Consequently, they act as X-ray absorbers predominantly in the second half of the orbit. In Vela X–1, an excess of absorption at late orbital phases is usually observed. This excess has been successfully modelled by means of the above-mentioned hydrodynamical simulations (Manousakis et al. 2012). That Vela X–1 and 4U 1538–522 are similar systems, since both have a donor of spectral type B0–0.5 I and very short orbital periods, implies that these structures are very likely to be present in 4U 1538–522.

Assuming that the eclipse egress ($\phi = [0.1–0.3]$) represents the unperturbed wind, the most precise value of \dot{M}/v_{∞} would be in the range $(0.3–1.0) \times 10^{-9} M_{\odot} \text{ yr}^{-1}/(\text{km s}^{-1})$. The median value of this range, namely $0.65 \times 10^{-9} M_{\odot} \text{ yr}^{-1}/(\text{km s}^{-1})$, is in excellent agreement with what was obtained by Clark et al. (1994). For the terminal velocities reported by Abbott (1982), this would translate into a mass loss of $(0.4–2.8) \times 10^{-6} M_{\odot} \text{ yr}^{-1}$ for QV Nor.

Nieuwenhuijzen & de Jager (1990) investigated the dependence of \dot{M} on the stellar fundamental parameters mass M , radius R , and luminosity L for a large sample of stars. They presented a simple parametrisation that gave a good description of observed mass-loss rates over the whole Hertzsprung-Russell diagram. We note that their formula has different numbers in the abstract than in the text, which we think are the correct ones. Therefore, we used the expression

$$\dot{M} = 9.55 \times 10^{-15} \left(\frac{L}{L_{\odot}} \right)^{1.24} \left(\frac{M}{M_{\odot}} \right)^{0.16} \left(\frac{R}{R_{\odot}} \right)^{0.81} M_{\odot} \text{ yr}^{-1}. \quad (2)$$

The astrophysical data for QV Nor are $\log(L/L_{\odot}) = 5.21 \pm 0.13$, $R/R_{\odot} = 17.2 \pm 1.0$, and $M/M_{\odot} = 20 \pm 4$ (Reynolds et al. 1992). By substituting these values into Eq. (2), the mass-loss rate was estimated as $\dot{M} = 4.5 \times 10^{-7} M_{\odot} \text{ yr}^{-1}$, in agreement with the lower value obtained by considering a spherically symmetric wind.

Our values also agree with the Abbott's correlation between mass-loss rate and luminosity, $\dot{M} = (0.03-1.0) \times 10^{-6} M_{\odot} \text{ yr}^{-1}$ (Abbott 1982). Finally, Clark et al. (1994) used a *Ginga* pointed observation to obtain a range $\dot{M} = (0.9-1.9) \times 10^{-6} M_{\odot} \text{ yr}^{-1}$ for the eclipse egress data, which is compatible with our estimation. Therefore, combining all the previous estimates, we can deduce a mass loss range for 4U 1538–52 of $\dot{M} = (1.2 \pm 0.7) \times 10^{-6} M_{\odot} \text{ yr}^{-1}$. These values would point to terminal wind velocities higher than 2000 km s^{-1} , so closer to the upper limit (2800 km s^{-1}) of the range derived by Abbott (1982).

5. Conclusions

From the analysis of the MAXI/GSC light curve, we estimated the orbital period of the binary system, $P_{\text{orb}} = 3.7285 \pm 0.0006$ days, which agrees with the best value derived by Mukherjee et al. (2006). From the unabsorbed flux, the X-ray luminosity in the 2–20 keV energy band was found: $L_X = (3.8 \pm 0.5) \times 10^{36} \text{ erg s}^{-1}$. We investigated the long-term orbital variation of spectral parameters doing an orbital phase-resolved spectroscopy of 4U 1538–52 with MAXI, so nearly five years of data. A higher value of \dot{M}/v_{∞} is clearly needed to fit the absorption column from orbital phases 0.4 into eclipse ingress. Using the N_{H} values up to orbital phase 0.3, which we consider the unperturbed wind, we measured the orbital dependence of the column density in the system and of the intrinsic source X-ray flux, and found that it was consistent on average with a spherically symmetric stellar wind from the optical counterpart of the binary system. We estimated the mass-loss rate range of the early-type B supergiant star QV Nor to be $\dot{M} = (1.2 \pm 0.7) \times 10^{-6} M_{\odot} \text{ yr}^{-1}$.

The slight asymmetric accretion column distribution between eclipse ingress and eclipse egress seen by MAXI was also found by RXTE and *BeppoSAX* (Mukherjee et al. 2006), suggesting that a trailing wake of material around the neutron star seems to be a permanent structure in this source.

Acknowledgements. We are grateful to the anonymous referee whose comments allowed us to improve this paper. Part of this work was supported by the Spanish Ministry of Economy and Competitiveness project numbers ESP2013-48637-C2-2P, and ESP2014-53672-C3-3-P, by the Vicerectorat d'Investigació, Desenvolupament i Innovació de la Universitat d'Alacant project number GRE12-35, and by the Generalitat Valenciana project number GV2014/088. This research made use of MAXI data provided by RIKEN, JAXA, and the MAXI team. J.J.R.R. acknowledges the support by the Matsumae International Foundation Research Fellowship No14G04, and also thanks the entire MAXI team for the collaboration and hospitality in RIKEN. The work of A.G.G. has been supported by the Spanish MICINN under FPI Fellowship BES-2011-050874 associated to the project AYA2010-15431. T.M. acknowledges the grant by the Vicerectorat d'Investigació, Desenvolupament i Innovació de la Universitat d'Alacant under visiting researcher programme INV14-11.

References

- Abbott, D. C. 1982, *ApJ*, **263**, 723
- Arnaud, K. A. 1996, in *Astronomical Data Analysis Software and Systems V*, eds. G. H. Jacoby, & J. Barnes, *ASP Conf. Ser.*, **101**, 17
- Baykal, A., Inam, S. Ç., & Beklen, E. 2006, *A&A*, **453**, 1037
- Becker, R. H., Swank, J. H., Boldt, E. A., et al. 1977, *ApJ*, **216**, L11
- Blondin, J. M., Kallman, T. R., Fryxell, B. A., & Taam, R. E. 1990, *ApJ*, **356**, 591
- Bulik, T., Riffert, H., Meszaros, P., et al. 1995, *ApJ*, **444**, 405
- Clark, G. W. 2000, *ApJ*, **542**, L131
- Clark, G. W., Woo, J. W., Nagase, F., Makishima, K., & Sakao, T. 1990, *ApJ*, **353**, 274
- Clark, G. W., Woo, J. W., & Nagase, F. 1994, *ApJ*, **422**, 336
- Corbet, R. H. D., Woo, J. W., & Nagase, F. 1993, *A&A*, **276**, 52
- Crampton, D., Hutchings, J. B., & Cowley, A. P. 1978, *ApJ*, **225**, L63
- Davison, P. J. N., Watson, M. G., & Pye, J. P. 1977, *MNRAS*, **181**, 73
- Dickey, J. M., & Lockman, F. J. 1990, *ARA&A*, **28**, 215
- Doroshenko, V., Santangelo, A., Nakahira, S., et al. 2013, *A&A*, **554**, A37
- Friend, D. B., & Abbott, D. C. 1986, *ApJ*, **311**, 701
- Hemphill, P. B., Rothschild, R. E., Caballero, I., et al. 2013, *ApJ*, **777**, 61
- Hemphill, P. B., Rothschild, R. E., Markowitz, A., et al. 2014, *ApJ*, **792**, 14
- Ilovaisky, S. A., Chevalier, C., & Motch, C. 1979, *A&A*, **71**, L17
- Islam, N., & Paul, B. 2014, *MNRAS*, **441**, 2539
- Kalberla, P. M. W., Burton, W. B., Hartmann, D., et al. 2005, *A&A*, **440**, 775
- Leahy, D. A. 1987, *A&A*, **180**, 275
- Makishima, K., Koyama, K., Hayakawa, S., & Nagase, F. 1987, *ApJ*, **314**, 619
- Manousakis, A., Walter, R., & Blondin, J. M. 2012, *A&A*, **547**, A20
- Matsuoka, M., Kawasaki, K., Ueno, S., et al. 2009, *PASJ*, **61**, 999
- Mihara, T., Nakajima, M., Sugizaki, M., et al. 2011, *PASJ*, **63**, 623
- Mukherjee, U., Raichur, H., Paul, B., Naik, S., & Bhatt, N. 2006, *JA&A*, **27**, 411
- Nakahira, S., Koyama, S., Ueda, Y., et al. 2012, *PASJ*, **64**, 13
- Nieuwenhuijzen, H., & de Jager, C. 1990, *A&A*, **231**, 134
- Prat, L., Rodriguez, J., Hannikainen, D. C., & Shaw, S. E. 2008, *MNRAS*, **389**, 301
- Rawls, M. L., Orosz, J. A., McClintock, J. E., et al. 2011, *ApJ*, **730**, 25
- Reynolds, A. P., Bell, S. A., & Hilditch, R. W. 1992, *MNRAS*, **256**, 631
- Robba, N. R., Cusumano, G., Orlandini, M., dal Fiume, D., & Frontera, F. 1992, *ApJ*, **401**, 685
- Robba, N. R., Burderi, L., Di Salvo, T., Iaria, R., & Cusumano, G. 2001, *ApJ*, **562**, 950
- Rodes, J. J., Torrejón, J. M., & Guillermo Bernabéu, J. 2008, in *The X-ray Universe 2008*, Symp., 56
- Rodes-Roca, J. J. 2007, Ph.D. Thesis, Dept. of Physics, Systems Engineering and Sign Theory, Univ. of Alicante
- Rodes-Roca, J. J., Torrejón, J. M., Kreykenbohm, I., et al. 2009, *A&A*, **508**, 395
- Rodes-Roca, J. J., Page, K. L., Torrejón, J. M., Osborne, J. P., & Bernabéu, G. 2011, *A&A*, **526**, A64
- Sugizaki, M., Mihara, T., Serino, M., et al. 2011, *PASJ*, **63**, 635
- Sunyaev, R. A., & Titarchuk, L. G. 1980, *A&A*, **86**, 121
- Titarchuk, L. 1994, *ApJ*, **434**, 570
- Tomida, H., Tsunemi, H., Kimura, M., et al. 2011, *PASJ*, **63**, 397
- Tsunemi, H., Tomida, H., Katayama, H., et al. 2010, *PASJ*, **62**, 1371
- Verner, D. A., Ferland, G. J., Korista, K. T., & Yakovlev, D. G. 1996, *ApJ*, **465**, 487
- Wilms, J., Allen, A., & McCray, R. 2000, *ApJ*, **542**, 914